15TH IEA HEAT PUMP CONFERENCE
MAY 26–29, 2026 | HOFBURG
VIENNA 2026
DECARBONISATION THROUGH INNOVATION

Preliminary design of an oil-cooled supercritical CO_2 heat exchanger for applications in high-temperature heat pumps

Emily Fricke[a,*], Zanil Narsing[a], Silvia Trevisan[a], Rafael Guedez[a]

[a]KTH Royal Institute of Technology, SE-100 44 Stockholm, Sweden

Abstract

There is a pressing need for industrial decarbonization, particularly in the area of process heating and cooling. Heat pumps with thermal energy storage (TES) can supply thermal energy for industrial processes and provide the opportunity to reduce fossil fuel use, with a growing interest in employing CO_2 as the working fluid in transcritical cycles to provide higher temperature heat. A key component impacting the overall performance of a CO_2 heat pump system is the heat sink, in which supercritical CO_2 rejects heat to a secondary fluid and interfaces with the hot TES. This work considers the preliminary design of the CO_2 cooler (i.e., the heat sink), in which CO_2 exchanges heat with thermal oil. In addition to developing a design with superior thermofluidic performance (i.e., high heat transfer and low pressure drops), the heat exchanger must withstand relatively high temperatures and pressures of up to 350 °C and 200 bar, respectively, on the CO_2 side. The thermofluidic performance of a hot and cold channel pair is evaluated via CFD, with the necessary channel wall thicknesses being assessed to ensure the mechanical robustness of the design. CFD is also used to evaluate the flow distribution from the header into the channels on the CO_2 side. The proposed channel design has an energy density of 5.6 MW/m^3, with pressure drops of 0.129 and 0.101 bar for the CO_2 and oil sides, respectively. The design is developed for later experimental characterization and integration into a heat pump test rig.

Selection and/or peer-review under the responsibility of the organizers of the 15th IEA Heat Pump Conference 2026.

Keywords: Printed circuit heat exchanger; supercritical CO_2 heat pump; heat sink; industrial decarbonization

1. Introduction

Developing and implementing systems that can provide decarbonized heating and cooling is critical. Heating is especially energy-intensive, comprising nearly half of global energy consumption, with industry accounting for 53% [1]. Fossil fuels are often employed to meet this need, with the share of renewables in industrial heat demand projected to reach just 13% by 2027 [1]. High-temperature heat pumps (HTHPs) have the potential to meet both heating and cooling needs, with the integration of TES enhancing viability. They also enable the integration of waste heat and renewables at various points in the cycle, either as temperature boosts or for electrical energy input. Although the potential of heat pumps (HPs) to provide heat for lower temperature applications (both residential and industrial) is widely recognized and implemented commercially, there is a growing interest in developing HTHPs that can deliver heat above 100 °C [2]. Transcritical cycles are promising in delivering higher temperature heat not limited by the critical point of the refrigerant. CO_2, with a critical point of 31.0 °C and 73.8 bar, has potential in transcritical cycles that allow it to operate beyond this point. In addition to being a safe, widely available, and low-cost refrigerant, CO_2 has superior heat transfer performance in its supercritical state that allows for more compact systems (exhibiting higher density and lower viscosity akin to the liquid and gas phases, respectively).

Various industrial applications require higher temperature heat. One potential application for HTHPs is in industrial drying, in which water is removed from a material. Spray drying in particular is a drying process in which hot air comes into contact with an atomized product, facilitating evaporation of excess water [3]. The

* Corresponding author.
E-mail address: efricke@kth.se

15th IEA Heat Pump Conference 2026 - ICO4.3 - https://doi.org/10.23697/3pqd-eq62

two outflow streams from the spray dryer are then the powdered product and the cooled, higher humidity air. Air for spray drying is typically supplied at 150-300 °C [3]. Spray drying is commonly used for making powdered dairy products such as whole milk powder, which typically requires heated air at 200-220 °C [3]. Various means can be used to heat the air, including steam, thermal oil, or an electric heater [3]. Process heat in the range of 100-200 °C accounts for 88% of the heat required to produce paper, and 100% of heat required for various basic chemicals such as polysulfones (commonly used for medical and laboratory equipment) ([4], [5]). Other applications in the food and beverage industry use heat in this temperature range, such as for brewing (where it accounts for 45% of the demand) and bread and baked goods (where it accounts for 33% of the heat demand, with 47% being accounted for by even higher temperatures ranging from 200-500 °C) [4].

High-temperature, high-pressure heat exchangers suitable for a working fluid of supercritical CO_2 (sCO_2) have been a topic of interest and research, especially for power cycle applications. Various reviews have examined developments in this field ([6], [7]). In a HTHP system, the heat sink or gas cooler must also be able to withstand high pressures and temperatures; in a system operating on a transcritical CO_2 cycle, this is the heat exchanger in which sCO_2 exiting the compressor is cooled by a sink fluid. In addition to thermal and hydraulic performance targets and requirements (high heat transfer rates and low pressure drops), cost, practicality, and feasibility must also be considered. Thus, heat exchanger design, material choice, and manufacturing methods are important factors. Commonly used high-temperature, high-pressure heat exchangers include printed circuit heat exchangers (PCHEs), diffusion-bonded plate fin heat exchangers (PFHEs), and micro shell and tube heat exchangers (MSTHEs) [6]. These designs are compact, allowing for higher power densities.

PCHEs are comprised of plates with photochemically etched channels for fluid flow. Due to the manufacturing process, the channels typically have a semicircular cross-section, with a depth (where the depth is the radius of the semi-circular channel) ranging from about 0.1 to 2.5 mm [8]. The plates are then diffusion bonded to form a strong, monolithic core. Diffusion bonding involves applying elevated pressures and temperatures to the pieces to be joined for a certain period of time [9]. It is a solid-state joining process that does not require filler material or liquid fusion. There has been investigation into various channels geometries that can increase the heat transfer beyond the traditional straight channels, such as zigzag or wavy channels. These enhance thermal performance at the cost of hydraulic performance, so discontinuous fin geometries such as s-shaped and airfoil fins to help mitigate pressure drop have been developed. Despite the potential for higher pressure drop, the zigzag channel geometry is more commonly employed as it provides a heat transfer enhancement over straight channels, and is easier to manufacture than discontinuous geometries (with challenges arising for these geometries due to the smaller area to be bonded on the plates) [7]. PCHEs present the most conventional option for higher pressure, higher temperature applications, with high compactness and robust and reliable performance up to 980 °C and 900 bar, with a specific area density of up to 2500 m^2/m^3 [10]. Due to the small channel sizes, they tend to have higher pressure drops. They are also more expensive because of the manufacturing methods employed, heavy, and prone to fatigue and fouling.

Despite these drawbacks, they offer various advantages over other heat exchanger types. PFHEs have lower compactness and robustness (with upper limits of around 1500 m^2/m^3 and 200 bar for surface area density and maximum pressure, respectively) [10]. Shell and tube heat exchangers are a conventional type of heat exchanger that, though inexpensive to manufacture and suitable for high-pressure operation, have low compactness, with a surface area density of up to 100 m^2/m^3 [10]. MSTHEs have been developed with smaller tube diameters on the order of 1 mm in an effort to enhance the surface area density of traditional shell and tube heat exchangers [7]. Although this allows for surface area densities on the order of those of PCHEs to be achieved, there are other drawbacks. Manufacturing issues can impact performance due to complications with joining the microtubes to the headers, which can lead to high pressure drops and blocked tubes.

Numerous studies on PCHEs have been performed. Some are concerned with developing correlations to characterize flow for different fluids and geometries from experimental or numerical data, although these are limited to the specific conditions for which the correlations were developed (fluid type, flow conditions, geometry details, etc.). Liu et al. (2020) experimentally examined flow in a PCHE in which sCO_2 is cooled by water to develop new flow correlations for friction factor and Nusselt number [11]. The PCHE had straight channels with a diameter of 1.87 mm. CO_2 conditions ranged from 7.53-11.97 MPa and 26.40-121.37 °C, with a bulk Reynolds number of 788-36700, while water conditions varied from 0.14-0.18 MPa and 23.10-90.96 °C, with a Reynolds number of 116-703. Saeed et al. (2020) also investigated as water-cooled sCO_2 PCHE, but developed correlations via a numerical study [12]. They investigated a zigzag channel PCHE, with a CO_2 inlet pressure of 8 MPa and 70 °C and a Reynolds number ranging from 3000 to 60000. Shi et al. (2020) developed correlations for a PCHE with airfoil fins employing either sCO_2 or MS on the hot side and synthetic oil on the cold side using a numerical model that they validated with prior experiments [13]. The sCO_2 and MS inlet temperatures ranged from 600 to 800 °C, with a pressure of 20 MPa being applied for the sCO_2 [13].

Other studies focus more on improvement and optimization of channel geometries. Saeed and Kim (2019) compared the performance of a zigzag PCHE to a design with sinusoidal fins, with sCO_2 as the heat transfer fluid [14]. Further optimization was then carried out on the design with sinusoidal fins using the response surface method (RSM) and a genetic algorithm to maximize the performance evaluation criteria, or PEC, which is a performance metric incorporating thermal and hydraulic performance (via Nusselt number Nu and friction factor f) relative to a baseline as

$$PEC = \frac{(Nu/Nu_{baseline})}{(f/f_{baseline})^{\frac{1}{3}}} \tag{1}$$

They found the pressure drop of the optimized design to be up to 2.5 times smaller than that of the zigzag geometry considered, with maximum and minimum PEC values ranging from 1.01-1.16 and 1.02-1.21 for both the hot and cold sides, respectively. Li et al. (2022) performed an optimization for a zigzag PCHE with supercritical methane as the working fluid, using RSM and considering the competing demands of thermal and hydraulic performance [15]. They varied channel diameter, longitudinal pitch, and bending angle for the optimization, finding 1.43mm, 24.6 mm, and 15° to result in the best performance.

Katz et al. (2021) performed an experimental study on a zigzag PCHE in which sCO_2 and helium exchanged heat [16]. Nominal operating conditions were inlet temperatures and pressures of 380 °C and 22 MPa for CO_2, and 550 °C and 3.3 MPa for helium. The Reynolds number varied from 370 to 17056 for CO_2 and from 390 to 3130 for helium. They developed flow correlations for Nusselt number and friction factor for both flows. When comparing the Nusselt numbers to those predicted from existing correlations in the literature, the observed values were higher. The authors noted shortcomings in some of the available correlations: a lack of clarity in how heat transfer surface areas are quantified that impact reproducibility, different methods for calculating hydraulic diameter (perpendicular to the direction of flow or perpendicular to the heat exchanger length), as well as instrumentation in experimental setups which did not separate the headers from the core, resulting in approximations needing to be made regarding header effects.

The header design is important to understand, not only in terms of sufficient instrumentation in experiments to isolate core and header performance, but also as an area for additional design refinement and optimization. Studies regarding core performance of PCHEs are more common than those investigating header design. For PCHEs, headers can be either externally welded on to the diffusion-bonded block, or they can be incorporated into the chemically etched plates. Note that externally welded headers necessitate cross-flow sections near the inlet and outlet regions for at least one of the flow paths, while integrated headers allow for a smaller non-counterflow section. Son et al. (2015) studied the impact of header flow path configuration on the core performance (in terms of effectiveness and pressure drop) for PCHEs with external, welded headers; their study highlighted the importance of accounting for these regions rather than approximating the performance with a purely counterflow model, which overestimates effectiveness and underestimates pressure drop [17]. Pasquier et al. (2016) studied the difference in distribution for four different types of headers for PCHEs, performing numerical simulations on the inlet and a short section of the channels, and studying the difference in flow velocity at the channel outlets [18]. They considered four types of headers (a trapezoidal header, a doubled header with bypass holes to aid in flow distribution, and two types of core-integrated headers), noting the competing demands of maintaining flow uniformity and minimizing the pressure drop. Zhang et al. (2022) studied the distribution of flow from the header into a set of plates, studying the impact of tapering the header on the flow distribution [19]. They found the optimum taper angle which maximized flow uniformity and, compared to the baseline design with no taper angle, enhanced the PEC by nearly 20%.

In this work, a PCHE design with a zigzag channel configuration is considered for greater potential commercializability and enhanced ease of manufacturing, with thermal oil as the sink fluid. The use of thermal oil is little-explored in the literature. Despite its higher cost, it provides more beneficial heat transfer properties than air. It also allows for higher temperature operation at atmospheric or near-atmospheric pressures in comparison to water, which must operate at higher pressure to maintain a liquid state at elevated temperatures. Having a sink fluid operating at higher pressures impacts not only the heat exchanger design, but also the design of the TES and piping on the sink side. Additional interfacing heat exchangers between the heat pump/TES and the process requiring heat can enable thermal oil to still be a viable heat transfer fluid. For example, with spray drying, sometimes thermal oil heaters are used to heat air, as previously mentioned. (Note that the details of any additional interfacing heat exchangers and TES, however, are beyond the scope of this work.) Additionally, due to its robustness at high pressures, the PCHE design presented could be viable for another sink fluid (such as water), with additional modifications as desired to the sink side to optimize the design for thermofluidic performance and mechanical integrity.

Additionally, the focus for PCHEs tends to be on core and channel design rather than header design. As such, the examination of a hybrid header design, with both integrated and externally welded headers, and the use of thermal oil as the sink fluid, will provide a useful addition to the existing literature. The header design enables more fully counterflow operation, and also presents a scalable design, whereas a design with integrated headers for both flow streams is more complicated to scale. The presented design uses an integrated header for the higher pressure fluid and a welded header for the lower pressure fluid, which prevents complications from requiring thick external headers to withstand high pressures on the CO_2 side.

2. Methodology

2.1. Application case and nominal boundary conditions

Nominal boundary conditions relevant to the high-temperature applications previously described were developed for the heat exchanger. They are included in Table 1. Note that the mass flowrate is given per cross-sectional area of the heat exchanger core.

Table 1. Nominal boundary conditions

Fluid	Inlet Temperature (°C)	Pressure (bar)	Mass flowrate (kg/m^2-s))
CO_2	240	200	20
Oil	50	1.01	10

2.2. Baseline PCHE design

Material selection is a key consideration for heat exchanger, particularly high-temperature, high-pressure ones. Although the heat exchanger is for a HTHP, a maximum design temperature of 350 °C is still relatively low in the realm of high-temperature, high-pressure heat exchangers. Hence, an iron-based alloy like stainless steel should be sufficient, rather than a nickel-based superalloy (or high-performance alloy) intended for more extreme operating conditions like Inconel. The 300-series formulas are widely used in the literature (e.g., 304, 316, and 316L), and are suitable for the lower temperatures considered [6]. The PCHE is assumed to be made out of stainless steel 316L. It is also a beneficial material to use since it is suitable for welding.

The PCHE plates are assumed to be 1.5 mm thick, which is readily available for manufacturing. The channel geometry is illustrated in Fig. 1, with values of the baseline design included in Table 2. The channel diameter is assumed to be 1.5 mm and the transverse pitch is 2.3 mm. These values were chosen based upon calculations to maintain the structural integrity of the plates. Channel dimensions and wall thicknesses can be determined based upon ASME Boiler and Pressure Vessel Code (BPVC), Section VIII, Appendix 13-9 (which includes information on stayed vessels of rectangular cross-section) [20]. The implementation of these equations for PCHE design is also described by Heatric [8]. In a conservative approach, the semi-circular channels are approximated as rectangular ducts with a height and width of $D/2$ and D, respectively. Note that the ultimate tensile strength and yield strength of SS316L are 485 MPa and 170 MPa, respectively, while the maximum allowable design stress at 350 °C is 94.1 MPa [21]. Further details are provided in Appendix A.

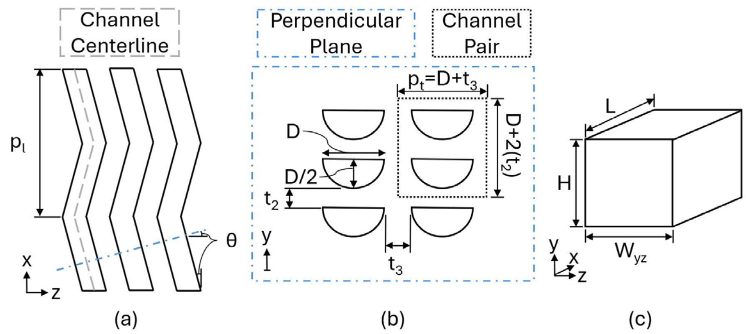

Figure 1. PCHE geometry for (a) the channels, (b) the cross-section perpendicular to the flow, and (c) the overall core.

Note that the channel path fillet radius listed in Table 2 is applied to the angles of the channel centerline shown in Fig. 1a. Table 2 includes the baseline values as well as the other values considered in brackets. Note that the core length used was determined from a preliminary 1D thermofluidic model for the PCHE to which the baseline geometric and flow parameters were applied. The length is the minimum value which allows a minimum pinch temperature of 10 °C to be obtained.

Table 2. Baseline geometric parameters and ranges for optimization

Parameter	Symbol	Value	Units
Diameter of semicircular channel	D	1.5	mm
Wall thickness	t_2	0.75	mm
Fin thickness	t_3	0.8	mm
Transverse pitch	p_t	2.3	mm
Longitudinal pitch	p_l	8	mm
Channel path fillet radius	-	0 [0, 1, 2]	mm
Zigzag angle	θ	40 [35, 40]	°
Core length	L	0.73	m

Fig. 2 shows the geometry of the plates and the fluid flow paths for a stack of plates forming the PCHE core. Note that the unit shown in Fig. 2b is for illustrative purposes, and has a shorter core length than that used for simulations. To this stack of plates, an additional end plate can be added to enclose the fluid flow in the top plate, and headers can be attached.

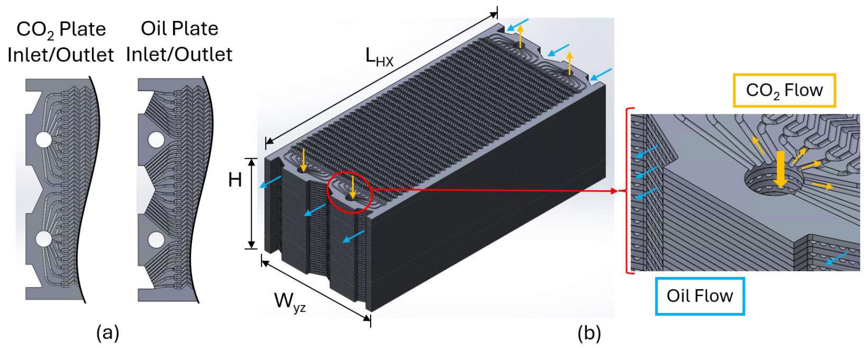

Figure 2. PCHE geometry showing (a) the plate inlets/outlets, and (b) the flow paths of the fluids in a stack of plates

For the baseline case, the PCHE performance was compared to a micro shell and tube heat exchanger (MSTHE), applying a 1D discretized model, with oil in the shell and CO_2 in the tubes. To reach the same thermal load, the MSTHE volume is 3.6 times the PCHE volume. Although the oil side pressure drop for the MSTHE was calculated to be about 1/10 the value for the PCHE, the CO_2 side pressure drop is 21% greater than it is with the PCHE. Thus, even with smaller tube sizes to enhance the heat transfer area of the traditional shell and tube heat exchanger, the larger volume and higher CO_2 pressure drop remain major drawbacks. Further details are included in Appendix C.

2.3. CFD model settings

Flow simulations were performed in ANSYS Fluent. For simulations on the PCHE core, a channel pair was modeled. Fig. 3 illustrates the model used along with some of the boundary conditions applied. Coupled walls were formed at the contacts between the metal walls and the fluid in the channel for both the CO_2 and the oil. A periodic condition was applied to the walls perpendicular to the y axis, illustrated in Fig. 3b (with the upper periodic face shown in red). For the zigzag walls (with those at the lower z location grouped together and those at the higher z location, shown in blue, grouped together), when the channel path was filleted, a periodic condition was applied, and when there was no fillet, the walls were assumed to be adiabatic. Both have been applied in the literature to PCHE channels, with researchers finding them to have good agreement [22]. The reason for the difference is because when the fillets were applied, the metal surrounding the fluid bodies still included a sharp zigzag to maintain the channel pair as a scalable unit, but the distance between the edge of the fluid channel and the outer wall is now different for the two sides, so an adiabatic (i.e., symmetric) condition can no longer be applied. For other walls (i.e., those of the extended fluid outlets, the metal faces perpendicular to the x direction), adiabatic boundary conditions were applied. The mesh included 12 inflation layers at the fluid walls, with a grid independence study being performed to ensure sufficient refinement. For the baseline case, increasing the refinement from 36.1 million elements to 48.2 million elements resulted in a percent difference in less than 0.2% for the fluid outlet temperatures and 1.3% for the pressure drops. Hence, the 36.1 million element mesh was used to minimize the computation time while maintaining reasonably refined results. The SST k-ω model was applied, with the mass flowrates and inlet temperatures being defined at mass flow inlets and pressure outlets being applied for the fluid outlets. Note that backflow temperatures were specified at the outlets, defined to be the inlet temperature of the other fluid. For the simulations, the residuals were at most on the order of 10^{-7} for energy, 10^{-5} for velocity, and 10^{-3} for turbulent kinetic energy and dissipation. The thermal oil was assumed to be Duratherm 600, which has a maximum operating temperature of 315 °C and temperature-dependent properties that were encoded in Fluent [23]. The NIST real gas model was applied to obtain property data for CO_2 in Fluent, with a lookup table being created with step sizes of about 0.33 K and 0.12 bar. 5 cm outlet extrusions were added for the fluids bodies to mitigate reverse flow.

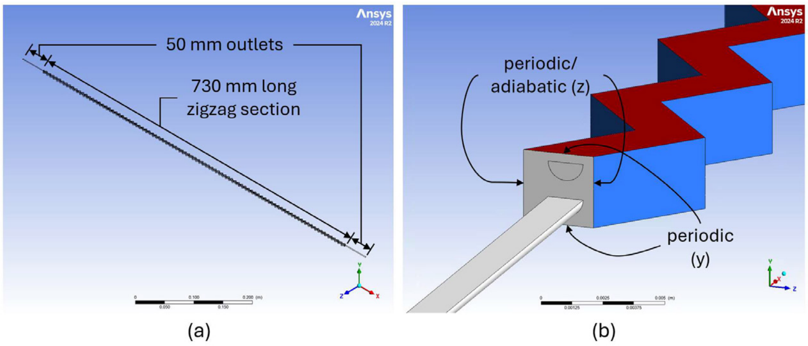

Figure 3. Geometry used for CFD on a channel pair showing (a) the channel pair, with extended outlets and (b) the boundary conditions applied to the edges of the metal.

The heat transfer rate q for one of the fluids of the channel pair can be obtained via the mass flow rate $\dot{m}$ and enthalpies h at the inlet and outlet as follows:

$$q = \dot{m}(h_{in} - h_{out}) \tag{2}$$

The average heat transfer rate can then be calculated based on the two flow streams.

Additionally, simulations were done to study the flow distribution from the CO_2 header into the channels. These were accomplished by taking pressure drop data for the PCHE channel with the optimal zigzag angle and fillet radius at a few mass flowrates and approximating the long zigzag channels as short (10 mm long) sections of porous media, which significantly reduces computation time. A flowrate of 4.32 g/s was used to meet the baseline flowrate for the 24 channels. The fluid mass flowrates at the outlets of each of the channels can then be recorded and compared. Fig. 4 shows the two geometries considered.

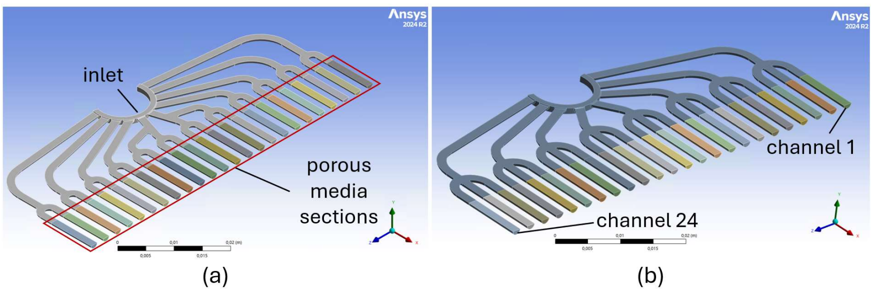

Figure 4. Geometry used for CFD on CO_2 plate header with (a) version 1 and (b) version 2 of the geometry.

3. Results and Discussion

3.1. Channel flow simulation

The key parameters that were varied were channel fillet and angle. Fig. 5a shows the impact of adding a fillet to the channel path for the baseline case on both average heat transfer rate and pressure drop. Adding a 1 mm fillet results in a heat transfer rate that is about the same as the case without the fillet; in fact, it is slightly higher at 37.1 W compared to 37.0 W with no fillet. It also reduces the pressure drop in both fluids albeit more significantly for the CO_2 (by 41% for CO_2 and 7.1% for oil). Further increasing the fillet to 2 mm results in another reduction in pressure drop (by 43% for CO_2 and 4.5% for oil), but also results in a 2.5% decrease in the heat transfer rate. Although the CO_2 pressure drop is significant, considering the fact that the CO_2 inlet pressure is 200 bar, for the case with the 1 mm fillet, the pressure drop of 0.129 bar is less than 0.1% of the overall pressure. The oil side pressure drop represents a more significant fraction of the fluid inlet pressure, at around 10% of the nominally atmospheric inlet pressure for the case with 1 mm fillets. However, as observed, the reduction in oil-side pressure drop is less significant as the fillet radius is increased. Hence, to maintain a higher heat transfer rate while mitigating the pressure drop, a fillet of 1 mm is selected. Fig. 5b shows the effect of channel zigzag angle upon thermofluidic performance. A smaller angle leads to a 1.32% drop in heat transfer, and also results in a reduction in pressure drop by 18.9% for CO_2 and 9.4% for oil. Despite the benefits in terms of pressure drop, the larger angle was selected to maintain the slightly higher heat transfer rate (keeping in mind that the baseline CO_2 pressure drop is only a little over 0.1% of the pressure drop at the larger angle). Note that for the case with varying zigzag angle, the same mass flowrates that were used for the 40° angle were applied (rather than scaling up the baseline values listed in Table 1 for the slightly altered cross-sectional area).

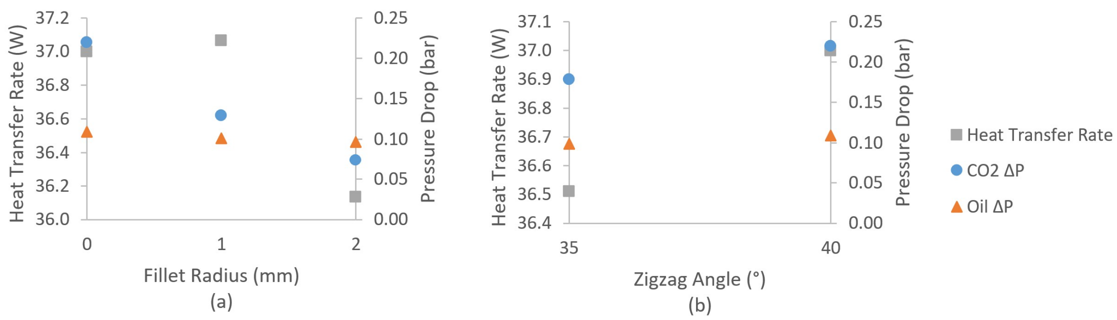

Figure 5. Variation in heat transfer rate and pressure drop for (a) a zigzag angle of 40° and varying fillet sizes and (b) no fillet and varying zigzag angles.

3.2. Header flow distribution

To compare the two versions of the CO_2 inlet header, two quantities are plotted in Fig. 6: the mass flowrate exiting each channel as well as the absolute deviation from the mean value expressed as a percentage (AD), defined for the ith channel as

$$AD_i = \frac{|\dot{m}_i - \dot{m}_{mean}|}{\dot{m}_{mean}} \times 100\% \tag{3}$$

where $\dot{m}_i$ is the mass flowrate exiting the ith channel and $\dot{m}_{mean}$ is the mean flowrate, the total inlet flowrate divided by the number of channels (0.180 g/s). Version 1, in an attempt to mitigate the effects of the shorter flow paths for channels most inline with the CO_2 header receiving the bulk of the flow, combines these channels prior to connecting them to the header. As can be seen from Fig. 6a, this leads to the lowest flows from these central channels. The maximum, minimum, and average values of the AD are 5.4%, 0.27%, and 2.2%, respectively. Version 2 of the header combines the channels in groups of 3 prior to joining with the header; as expected, the channels most inline with the CO_2 header exhibit higher flows, while the outer channels have lower flows. Here, the maximum, minimum, and average values of the AD are 4.8%, 0.66%, and 2.3%, respectively. Hence, the maximum deviation has been slightly reduced, but the minimum and average deviations are slightly higher. Given that the maximum deviation has been reduced below 5%, the second version is more desirable than the first, but further refinement could help even the flow distribution more. The difference in predicted pressure drop is also worth noting; version 2 is accompanied by a slight increase in pressure drop, but the percent increase relative to the pressure drop in version 1 is only 1.33%. Compared to the core simulation, the pressure drop accounting for the inlet region is about 10% higher. Although this is significant, the overall pressure drop is still expected to be less than 0.1% of the CO_2 inlet pressure.

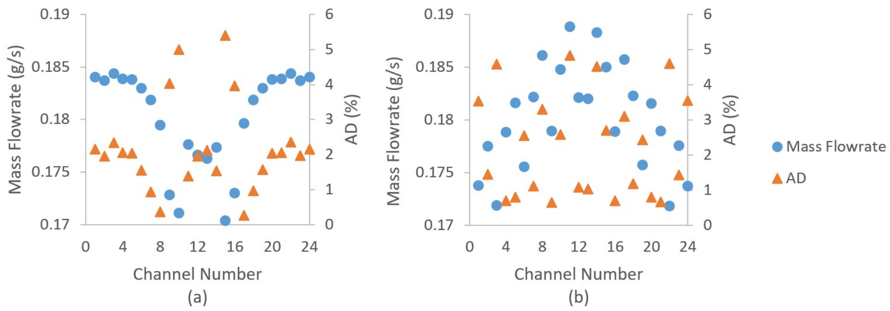

Figure 6. Variation in mass flowrate and *AD* for the various CO_2 channels for (a) the first version of the header geometry (b) the second version of the header geometry.

3.3. Scale-up considerations

Considering the baseline case with the optimal channel fillet and angle, if a nominally 0.5 MW heat exchanger is desired, the heat exchanger cross-sectional area needed to meet the load is 0.122 m^2, or 0.35 x 0.35 m. The developed design is suitable for upscaling in the y and the z directions (i.e., in both the height and the width). To scale up in the z direction, additional CO_2 inlet/outlet pairs can be added beyond the two shown in Fig. 2. To scale up in the y direction, more plates can be added to the PCHE. Additionally, if higher flowrates are desired, another upscaling option could be to increase the heat exchanger length.

4. Conclusions

This paper presented the preliminary design of a PCHE suitable for cooling supercritical CO_2 with thermal oil, designed to handle temperatures up to 350 °C and pressures up to 200 bar on the CO_2 side. For the optimal channel fillet and zigzag angle of 1 mm and 40°, respectively, a heat transfer rate of 37.1 W was achieved by a channel pair, with pressure drops of 0.129 bar and 0.101 bar on the CO_2 and oil sides, respectively. For this optimal channel, simulations were done on a few different CO_2 header designs to examine the impact upon flow distribution, with a maximum absolute deviation in channel mass flowrate of below 5% being achieved. Further work could be done on the header distribution, as well as verification of the mechanical integrity of the header via static structural simulations. Additional optimization could be performed on the channel geometry, e.g., studying the impact of varying longitudinal pitch on the thermofluidic performance.

Acknowledgements

This research was funded by CETPartnership, the Clean Energy Transition Partnership under the 2023 joint call for research proposals, co-funded by the European Commission (GA N°101069750) and with the funding organizations detailed on https://cetpartnership.eu/funding-agencies-and-call-modules. The project has received support from the Swedish Energy Agency, Scottish Enterprise, and the CDTI.

References

[1] IEA (2022), Renewables 2022, IEA, Paris https://www.iea.org/reports/renewables-2022, License: CC BY 4.0.

[2] Adamson, K.-M., Walmsley, T. G., Carson, J. K., Chen, Q., Schlosser, F., Kong, L., & Cleland, D. J. (2022). High-temperature and transcritical heat pump cycles and advancements: A review. *Renewable and Sustainable Energy Reviews, 167*. https://doi.org/10.1016/j.rser.2022.112798.

[3] Tetra Pak. (2025). Dairy Processing Handbook. https://dairyprocessinghandbook.tetrapak.com/.
[4] Rehfeldt, M., Fleiter, T., & Toro, F. (2018). A bottom-up estimation of the heating and cooling demand in European industry. *Energy Efficiency 11,* 1057–1082. https://doi.org/10.1007/s12053-017-9571-y.
[5] Fan, J., & Njuguna, J. (2016). 1 - An introduction to lightweight composite materials and their use in transport structures. In J. Njuguna (Ed.), *Lightweight Composite Structures in Transport* (pp. 3-34). Woodhead Publishing. https://doi.org/10.1016/B978-1-78242-325-6.00001-3.
[6] Chai, L., & Tassou, S. A. (2023). Recent Progress on High Temperature and High Pressure Heat Exchangers for Supercritical CO_2 Power Generation and Conversion Systems. *Heat Transfer Engineering, 44*(21–22), 1950–1968. https://doi.org/10.1080/01457632.2022.2164683.
[7] Kwon, J. S., Son, S., Heo, J. Y., & Lee, J. I. (2020). Compact heat exchangers for supercritical CO_2 power cycle application. *Energy Conversion and Management, 209*. https://doi.org/10.1016/j.enconman.2020.112666.
[8] Le Pierres, R., Southall, D., & Osborne, S. (2011). Impact of Mechanical Design Issues on Printed Circuit Heat Exchangers. *Proceedings of the SCO_2 Power Cycle Symposium*, Boulder, CO, USA.
[9] Sundén, B., & Fu, J. (2017). *Heat transfer in aerospace applications.* Academic Press.
[10] Zhang, X., Keramati, H., Arie, M., Singer, F., Tiwari, R., Shooshtari, A., & Ohadi, M. (2018). Recent Developments in High Temperature Heat Exchangers. *Frontiers in Heat and Mass Transfer, 11,* 1-14. https://doi.org/10.5098/hmt.11.18.
[11] Liu, S. Huang, Y., Wang, J., Liu, R., & Zang, J. (2020). Experimental study of thermal-hydraulic performance of a printed circuit heat exchanger with straight channels. *International Journal of Heat and Mass Transfer, 160.* https://doi.org/10.1016/j.ijheatmasstransfer.2020.120109.
[12] Saeed, M., Berrouk, A. S., Siddiqui, M. S., & Awais, A. A. (2020). Numerical investigation of thermal and hydraulic characteristics of sCO_2-water printed circuit heat exchangers with zigzag channels. *Energy Conversion and Management, 224.* https://doi.org/10.1016/j.enconman.2020.113375.
[13] Shi, H.-Y., Li, M.-J., Wang, W.-Q., Qiu, Y., & Tao, W.-Q. (2020). Heat transfer and friction of molten salt and supercritical CO_2 flowing in an airfoil channel of a printed circuit heat exchanger. *International Journal of Heat and Mass Transfer, 150.* https://doi.org/10.1016/j.ijheatmasstransfer.2019.119006.
[14] Saeed, M., & Kim, M.-H. (2019). Thermal-hydraulic analysis of sinusoidal fin-based printed circuit heat exchangers for supercritical CO_2 Brayton cycle. *Energy Conversion and Management, 193,* 124-139. https://doi.org/10.1016/j.enconman.2019.04.058.
[15] Li, Y., Li, Q., Wang, Y., Chen, J., & Cai, W.-H. (2022). Optimization of a Zigzag-channel printed circuit heat exchanger for supercritical methane flow. *Cryogenics, 121.* https://doi.org/10.1016/j.cryogenics.2021.103415.
[16] Katz, A., Aakre, S. R., Anderson, M. H., & Ranjan, D. (2021). Experimental investigation of pressure drop and heat transfer in high temperature supercritical CO_2 and helium in a printed-circuit heat exchanger. *International Journal of Heat and Mass Transfer, 171.* https://doi.org/10.1016/j.ijheatmasstransfer.2021.121089.
[17] Son, S., Lee, Y., & Lee, J. I. (2015). Development of an advanced printed circuit heat exchanger analysis code for realistic flow path configurations near header regions. *International Journal of Heat and Mass Transfer, 89,* 242-250. https://doi.org/10.1016/j.ijheatmasstransfer.2015.05.012.
[18] Pasquier, U., Chu, W. X., Zeng, M., Chen, Y. T., Wang, Q. W., & Ma, T. (2016). CFD simulation and optimization of fluid flow distribution inside printed circuit heat exchanger headers. *Numerical Heat Transfer, Part A: Applications, 69*(7), 710–726. https://doi.org/10.1080/10407782.2015.1090771.
[19] Zhang, K., Wei, W., Sun, Y., Wu, Q., Tang, M., & Lu, M. (2022). Design and Optimization of the Inlet Header Structure in Microchannel Heat Exchanger Based on Flow Distribution Uniformity. *Applied Sciences, 12*(13), 6604. https://doi.org/10.3390/app12136604.
[20] American Society of Mechanical Engineers. (2023). *2023 ASME Boiler and Pressure Vessel Code, Section VIII, Division 1.* American Society of Mechanical Engineers (ASME).
[21] American Society of Mechanical Engineers. (2023). *2023 ASME Boiler and Pressure Vessel Code, Section II - Materials.* American Society of Mechanical Engineers (ASME). Retrieved on October 21, 2025 from https://app.knovel.com/hotlink/toc/id:kpASMEBPC1/asme-boiler-pressure/asme-boiler-pressure.
[22] Li, Y., Li, Q., Wang, Y., Chen, J., & Cai, W.-H. (2022). Optimization of a Zigzag-channel printed circuit heat exchanger for supercritical methane flow. *Cryogenics, 121.* https://doi.org/10.1016/j.cryogenics.2021.103415.
[23] Duratherm. *Duratherm 600 Technical Data Sheet.* Retrieved September 18, 2025 from https://durathermfluids.com/pdf/productdata/heattransfer/duratherm-600.pdf.

[24] Hesselgreaves, J. E. (2001). Compact Heat Exchangers: Selection, Design and Operation. Elsevier.
[25] Nellis, G. F., & Klein, S. A. (2009). Heat transfer. Cambridge University Press.
[26] Chai, L., & Tassou, S. A. (2021). Modeling and Evaluation of the Thermohydraulic Performance of Compact Recuperative Heat Exchangers in Supercritical Carbon Dioxide Waste Heat to Power Conversion Systems. *Heat Transfer Engineering, 43*(13), 1067–1082. https://doi.org/10.1080/01457632.2021.1943833.

Appendix A: Mechanical Integrity Calculations

The required wall thicknesses can be calculated based upon the maximum allowable stress, S, using the equations outlined in ASME BPVC, Appendix 13-9 [20]. Note that in addition to determining t_2 and t_3, pictured in Fig. 1, another thickness, t_1, is calculated, which is parallel to t_3, but is the thickness at the outside of the heat exchanger rather than between adjacent channels. For stainless steel 316L at 350 °C, S is 94.1 MPa (from Table 1A of the ASME Boiler and Pressure Vessel Code, Section II - Materials) [21]. This allowable stress value is the minimum value calculated based on a variety of considerations included in Mandatory Appendix 1 (such the tensile strength divided by 3.5, 2/3 of the yield strength). Creep and stress rupture are also taken into consideration, with other potential values of the maximum allowable stress being the average stress required to produce creep at a rate of 0.01%/1000 h, 80% of the minimum stress to result in rupture after 100 000 h, and the average stress to cause rupture at the end of 100 000 h multiplied by a factor of 0.67 [21]. Note that the ultimate tensile strength and yield strength are 485 MPa and 170 MPa, respectively. Two key metrics to be calculated for the various thicknesses (t_1, t_2, and t_3) are the membrane and bending stresses (S_m and S_b, respectively). For each dimension, the membrane stress must be below SE and the total stress must be below $1.5SE$, where E is the joint factor (with 0.7 being used for the PCHE based on the value given by Heatric [8]). Note that K, the vessel parameter, is assumed to be zero for these equations (which holds when $I_1 >> I_2$). Note that P is the design pressure, for which a pressure of 220 bar is used (10% above the expected maximum operating pressure of 200 bar). In the equations, h and H are used in place of D and $D/2$, respectively.

The equations governing the value of t_1 are as follows:

$$S_m = \frac{Ph}{2t_1} \tag{4}$$

$$(S_b)_N = \frac{Pc}{24I_1}(2h^2 - 3H^2) \tag{5}$$

$$(S_b)_Q = \frac{Ph^2c}{21I_1} \tag{6}$$

where $c = (t_1)/2$ and $I_1 = (t_1)^3/12$. The total stresses can then be calculated as

$$(S_T)_N = S_m + (S_b)_N \tag{7}$$

$$(S_T)_Q = S_m + (S_b)_Q \tag{8}$$

The equations governing the value of t_2 are as follows:

$$S_m = \frac{PH}{2t_2} \tag{9}$$

$$(S_b)_M, (S_b)_Q = S_b = \frac{Ph^2c}{12I_2} \tag{10}$$

where $c = (t_2)/2$ and $I_2 = (t_2)^3/12$. Note that the two bending stresses are calculated using the same equation. Hence, the total stress can be calculated as

$$(S_T)_M, (S_T)_Q = S_T = S_m + S_b \tag{11}$$

The equations governing the value of t_3 are as follows (note that the bending stress is zero):

$$S_m = \frac{Ph}{t_3} \tag{12}$$

$$S_T = S_m \tag{13}$$

Based upon these equations, minimum values of t_1=5 mm, and t_2, t_3=0.55 mm are acceptable. However, given the plate thickness of 1.5 mm, t_2 will be 0.75 mm. For enhanced integrity, t_3=0.8 mm is used.

Appendix B: Thermofluidic Model

A 1D thermofluidic model was developed to model the PCHE core performance. The model considers a unit cell in the cross-section, comprised of half of a CO_2 channel, half of an oil channel, and the wall between in the height, with the unit cell width equal to the transverse pitch. This is discretized into control volumes (CVs) along the length, as shows in Fig. 7.

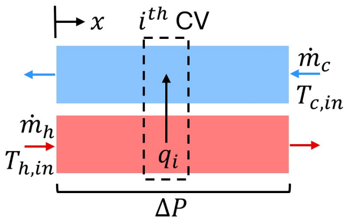

Figure 7. Discretized unit cell for PCHE model.

The heat transferred from the hot fluid to the cold fluid in the i[th] CV q_i can be calculated using mass flowrate $\dot{m}$, enthalpy h, specific heat c_p, and temperature T, using the following equations:

$$q_i = \dot{m}_h(h_{h,i} - h_{h,i+1}) \tag{14}$$

$$q_i = \dot{m}_c c_{p,i}(T_{c,i} - T_{c,i+1}) \tag{15}$$

$$q_i = \frac{(T_{h\,avg,i} - T_{c\,avg,i})}{R_{tot,i}} \tag{16}$$

Note that the subscripts are used to denote the fluid (with *h* referring to the hot CO_2 stream and *c* referring to the cold oil stream), as well as the CV (for properties such as specific heat, which are taken using the average temperature across the CV, $T_{avg,i}$) or the node (e.g., for enthalpy and temperature). $R_{tot,i}$ is the total thermal resistance, which is the sum of three resistances: conductive resistance through the wall, and convective resistances on the CO_2 and oil sides. Conductive and convective resistances R_{cond} and R_{conv} can be calculated as

$$R_{cond} = \frac{t}{kA} \tag{17}$$

$$R_{conv} = \frac{1}{htcA} \tag{18}$$

where t is wall thickness, k is the thermal conductivity, A is the relevant heat transfer area, and htc is the convective heat transfer coefficient. The heat transfer coefficient is calculated in terms of the Nusselt number Nu and hydraulic diameter D_h as

$$htc = \frac{Nuk}{D_h} \tag{19}$$

The Nusselt number and friction factor can be determined by relevant correlations as functions of Reynolds number Re and Prandtl number Pr. For CO_2, the correlations from Saeed et al. (2020) are applied, which are developed for $3000 \leq Re \leq 60000$ and $2.0 \leq Pr \leq 13$ [12].

$$Nu = 0.475Re^{0.61}Pr^{0.17} \tag{20}$$

$$f = 0.13Re^{-0.044} \tag{21}$$

For oil, the correlations developed by Hesselgreaves (2001) for various fluids flowing in straight, semicircular channels with $Re \leq 2300$ were applied [24].

$$Nu = 4.089 \tag{22}$$

$$f = \frac{15.78}{Re} \tag{23}$$

The pressure drop ΔP can then be calculated based as

$$\Delta P = f\frac{L}{D_h}\frac{1}{2}\rho V^2 \tag{24}$$

where L is the length of the flow path, ρ is the density, and V is the velocity.

Appendix C: Comparison to MSTHE

A model of a MSTHE was developed to compare against the PCHE model described in Appendix B. A model similar to that described in Appendix B can be developed, applying appropriate correlations for the Nusselt numbers and friction factors. In this case, the unit cell is a square area in the cross section with a side length equal to the pitch between the tubes. For both fluid streams, for Reynolds numbers in excess of 2300, the Gnielinski correlation (relevant for $0.5 < Pr < 2000$ and $2300 < Re < 5\ x\ 10^6$) is used to obtain Nusselt number and the correlation developed by Petukhov (1970) for $3000 < Re < 5\ x\ 10^6$ is applied to calculate friction factor, as tabulated by Nellis and Klein (2009) [25].

$$Nu = \frac{\frac{f}{8}(Re-1000)Pr}{1+12.7\left(Pr^{2/3}-1\right)\sqrt{f/8}} \tag{25}$$

$$f = (0.790\,ln(Re) - 1.64)^{-2} \tag{26}$$

These turbulent correlations were likewise applied by Chai and Tassou (2021) in their comparison of various recuperative sCO_2 heat exchangers [26]. For laminar flow with $Re \leq 2300$, Nu and f are approximated using the correlations for flow in a circular duct, averaging the constant wall temperature and constant heat flux case values to obtain Nu.

$$Nu = 4.01 \tag{27}$$

$$f = \frac{64}{Re} \tag{28}$$

For the MSTHE, the tubes are assumed to have an inner diameter of 1 mm, 0.5 mm walls, and equal transverse and vertical pitches of 3 mm. As with the PCHE model, only the core is considered, where flow is assumed to be counterflow. The flow rates per cross-sectional area are the same.

Fixing the PCHE cross-sectional area at 0.25 m x 0.25 m, the total heat transfer achieved with the length of 0.73 m is 256 kW, with pressure drops of 7.00 kPa and 3.01 kPa across the CO_2 and oil, respectively. For the same cross-sectional area, a length of 2.6 m for the MSTHE is required to achieve the same heat transfer rate. The pressure drops across CO_2 and oil, respectively, are 8.47 kPa and 0.303 kPa.